ASPECTS OF MODELLING A COMPLEX CHLORIDE LEACH CIRCUIT: STARFIELD RESOURCES' FERGUSON LAKE PROJECT

by

Mike Dry

Arithmetek Inc. Ontario, Canada

mdry3@cogeco.ca

ABSTRACT

The enabling step in a chloride-based circuit being developed for processing bulk sulphide ore from Starfield Resources' Ferguson Lake deposit is the hydrolysis of ferric chloride to hematite and hydrochloric acid, the acid being recycled and the hematite being an environmentally friendly stable residue. The chemistry and thermodynamics relevant to the hydrolysis step were modeled and the results were used to generate an overall mass/energy balance for the circuit. This paper presents selected aspects of the modeling work.

CONTENTS

1. INTRODUCTION

A novel hydrometallurgical process has been developed by NeoFerric Technologies Inc. for Starfield Resources' Ferguson Lake Project in Nunavut, Canada[1,2,3]. A recent metallurgical scoping study[4] by Scott Wilson RPA indicates that the project is economically attractive, even though it is situated in a remote location with no infrastructure and has relatively low head grades of nickel and copper. A major facet of this project's economic viability is that it is a net producer of energy and does not need significant amounts of fossil fuel. Modelling of the mass and energy balance around the circuit played a pivotal role in its development. This paper focuses on selected aspects of the modelling exercise.

The process is based on highly concentrated chloride solutions. Chloride hydrometallurgy has two useful facets to its chemistry, *viz.*

- In concentrated chloride solutions the activity of hydrochloric acid is elevated relative to the same nominal acid concentration in water.
- In sufficiently concentrated chloride solutions at high enough temperatures, the volatility of hydrochloric acid is significantly elevated and ferric chloride can be decomposed to hematite and hydrogen chloride. This is referred to as the hydrolysis of ferric chloride. The acid can be recovered as a gas and recycled, essentially eliminating the overall consumption of acid in the circuit and also avoiding the addition of neutralizing reagent to precipitate the iron.

The associated cost is that of energy. For essentially complete hydrolysis, the chemistry requires temperatures in the general vicinity of 200°C. The molten slurry has to be filtered, the filter cake has to be washed with water to separate it from the residual chloride and the wash filtrate has to be recycled to preserve the overall chloride balance. Heating the chloride brine back up to the hydrolysis temperature after the other process steps (leaching, etc.) entails boiling as the wash water evaporates, consuming energy.

In the case of low grade sulphide ores such as nickeliferous pyrrhotite, the ore itself can be used, albeit indirectly, as a fuel if the sulphide sulphur can be converted to sulphuric acid. An application of this approach, currently under development for Starfield Resources Inc., is a circuit for the processing of bulk low-grade sulphide ore from the Ferguson Lake Deposit in Nunavut, Canada. Figure 1 is a conceptual diagram of this circuit. The full details are given elsewhere[3,4], but in essence the circuit entails the following process steps, all done in a background of concentrated magnesium chloride.

- Leaching the ore with hydrochloric acid, producing hydrogen sulphide and ferrous chloride.
- Oxidizing the ferrous chloride to ferric chloride and precipitating one third of the iron as hematite.
- Leaching the residue from the non-oxidative leach with some of the ferric chloride to dissolve the base metals.
- Evaporation to raise the boiling point of the ferric chloride solution not used to leach the residue from the non-oxidative leach.
- Hydrolysis of the concentrated ferric chloride to hematite and hydrochloric acid.

- Converting the hydrogen sulphide to sulphuric acid, releasing the energy needed to drive the evaporation and hydrolysis steps.
- Recovery of the base metals from the solution ex the oxidative leach.

Figure 1 – Conceptual diagram

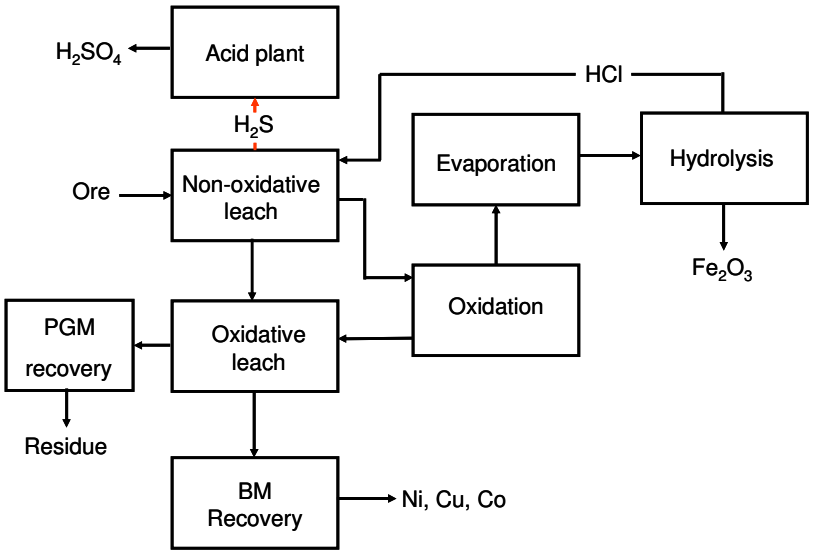

The block labeled hydrolysis, in which the ferric chloride is converted to crystalline hematite and hydrogen chloride that is recovered from the gaseous phase and recycled, is the step that enables this concept. The evaporation stage is there to concentrate the chloride solution to a high enough boiling point for the hydrolysis reaction to proceed essentially to completion.

Process modeling has been used to facilitate the development of this concept, enabling the logical extrapolation of results from laboratory work to a mass/energy balance that in turn led to an optimized provisional overall energy balance and enabled estimation of the capital and operating costs potentially associated with the Starfield circuit to a significantly higher level of confidence than would otherwise have been possible, thereby justifying its ongoing development.

This work used a steady-state process simulation package known as AspenPlus®.

2. CHEMISTRY

The crux of the novel technology being the hydrolysis of ferric chloride to Fe_2O_3 and HCl, the process model requires a plausible representation of the relevant chemistry. The liquid phase after hydrolysis is more a melt of hydrated magnesium chloride than an aqueous solution of magnesium chloride and the gas phase over this melt contains H_2O and HCl in equilibrium with the melt, putting this system well outside the range of solutions usually used in hydrometallurgical processing. Generally, the higher the temperature the less reliable any properties extrapolated from available data generated at lower temperatures, therefore the ideal situation would be to base the model on appropriate high-temperature data. This has been partially achieved, in that applicable published data was found for the H_2O-$MgCl_2$ system. The basic binary systems of interest are H_2O-HCl and H_2O-$MgCl_2$. A tertiary system of interest is H_2O-HCl-$MgCl_2$.

2.1. $HCl\text{-}H_2O$

It is well known that the HCl-water system exhibits azeotropic behavior in its vapor-liquid equilibrium. Hydrochloric acid dissociates in water, as follows.

$$HCl + H_2O \leftrightarrow H_3O^+ + Cl^-$$

In dilute solutions the acid is very nearly completely dissociated, but in more concentrated solutions HCl appears as a distinct species. The HCl molecule is more volatile than water, which gives rise to the behavior of this system. As a dilute solution of hydrochloric acid in water is evaporated, at first the vapor phase contains essentially only water because practically all of the hydrochloric acid has dissociated into non-volatile ionic H_3O^+ and Cl^-. As the remaining solution becomes more concentrated in chloride ions the dissociation equilibrium shifts towards molecular HCl that is more volatile than water. As the concentration of molecular HCl increases, relatively more of it enters the vapor phase, until the liquid and the vapor contain the same proportions of H_2O and HCl. This is referred to as an azeotropic composition. Figure 2 is a plot of vapor-liquid equilibrium in the HCl-water system. The dotted line shows where the compositions of the vapor and liquid phases are equal and the black dots are measured data[5]. The curves were generated from a template in the AspenPlus® library.

Figure 2 – $HCl\text{-}H_2O$ equilibrium

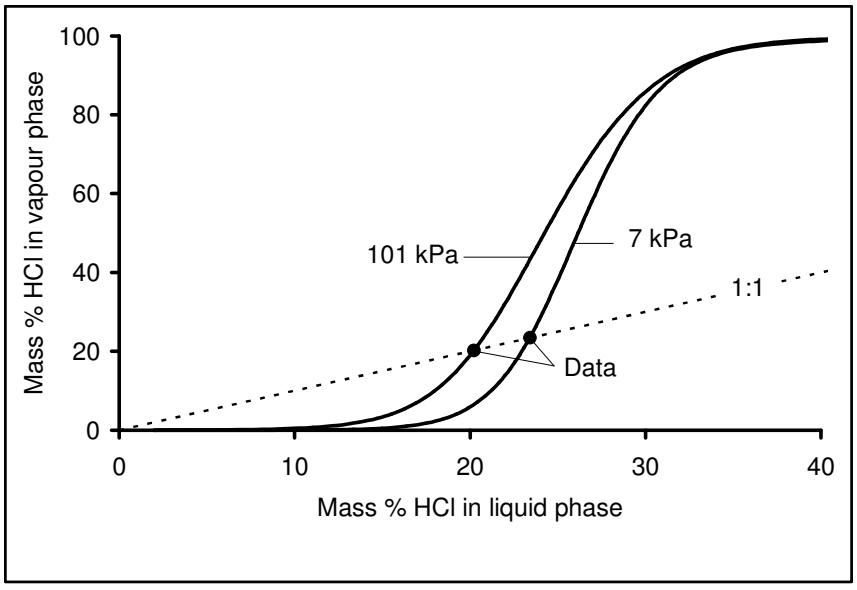

The purpose of Figure 2 is merely to show that the software used in this work can be used to accurately reproduce vapor-liquid equilibrium data in the HCl-water system over the composition range shown.

2.2. $MgCl_2\text{-}H_2O$

Wendt *et al.* presented a semi-empirical correlation of the thermodynamic properties of molten mixtures of water and magnesium chloride[6]. Figure 3 shows the fit between this correlation and measured data[7], for the partial pressure of water over molten mixtures of magnesium chloride and

water. The values of n refer to the molar ratio of water to magnesium chloride in the liquid phase. The temperature range spanned by the data is 129ºC to 228ºC.

Figure 3 – H_2O-$MgCl_2$ equilibrium

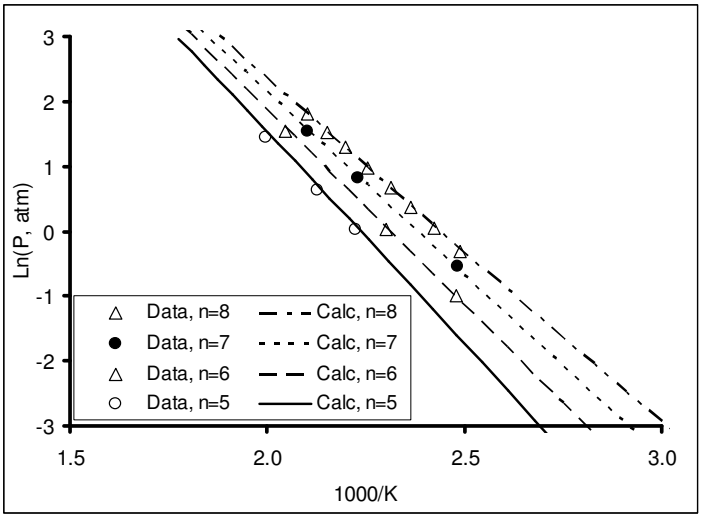

The correlation in Wendt *et al.*'s paper was used to generate vapor-liquid equilibrium (VLE) data at atmospheric pressure for the H_2O-$MgCl_2$ system. The results are shown in Table 1. The thermodynamic correlations in AspenPlus® were calibrated to these numbers.

Table 1 – Data generated for molten $MgCl_2 \cdot nH_2O$

H_2O:$MgCl_2$ molar ratio, n	Boiling point ºC	Enthalpy, kcal/mol	
		$MgCl_2 \cdot nH_2O$	H_2O (Vapor)
25.0	100.9	-1862.6	-57.99
21.3	101.4	-1614.4	-58.00
12.1	112.9	-1004.5	-58.01
8.0	137.1	-726.1	-58.02
7.0	147.6	-656.7	-58.03
6.8	150.0	-642.4	-58.04
6.0	160.5	-586.5	-58.06
5.0	176.3	-515.0	-58.07
5.1	175.0	-520.3	-58.08
4.0	195.4	-442.2	-58.09
3.1	200.0	-426.3	-58.10
3.5	206.4	-405.2	-58.11
3.0	218.3	-367.8	-58.12

Figure 4 shows the atmospheric boiling point *versus* temperature predicted by the software after calibration and the same data from Wendt *et al.'s* correlation. The single triangular symbol in this graph is a data point measured at McGill University as part of the experimental work done so far. This plot shows that the process model was successfully calibrated to predict the atmospheric boiling point of mixtures of water and magnesium chloride up to the temperature required for the

hydrolysis of ferric chloride. Figure 5 shows the fit between the calibrated model and different data generated at McGill University, for $MgCl_2$ in water at molalities of 1.05 and 4.1.

Figure 4 – Boiling point versus melt composition

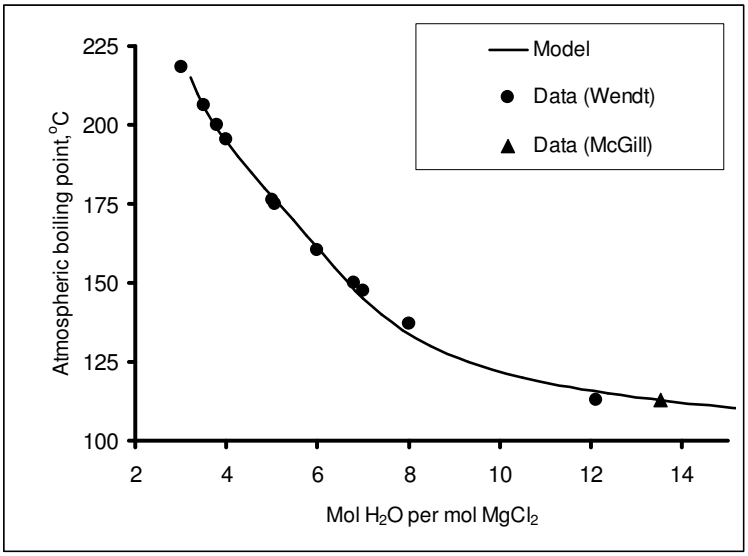

Figure 5 – H_2O pressure over solutions of $MgCl_2$

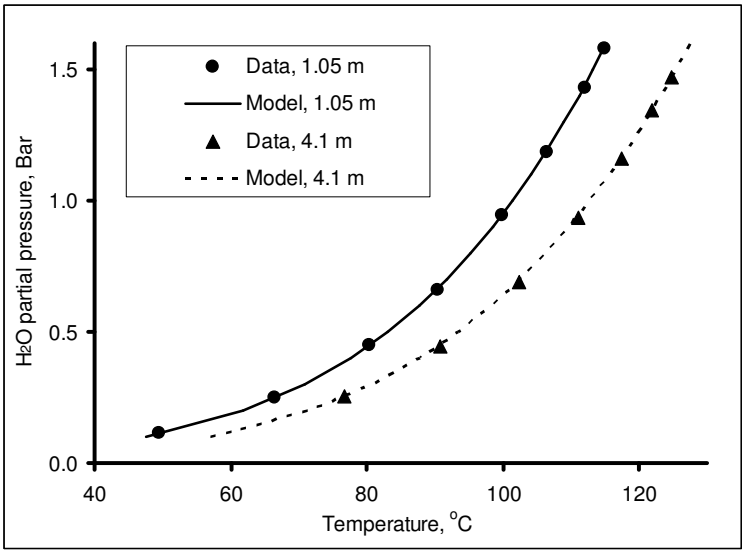

Figure 6 shows the energy required to evaporate the water from a solution initially containing 25 moles of water per mol of $MgCl_2$, plotted against the molar ratio of water to magnesium chloride in the final melt. Figure 7 plots the same data, but against the atmospheric boiling point of the final melt. The calibrated software over-estimates the energy requirement somewhat. Above about 140ºC the slope of the model prediction is very similar to that of Wendt *et al.*'s correlation, so the deviation occurs below that temperature. This is a topic for future work, but at this stage over-estimation of the energy for evaporation probably represents a small margin of safety for the overall economics associated with this chemistry.

Figure 6 – Evaporation energy versus melt composition

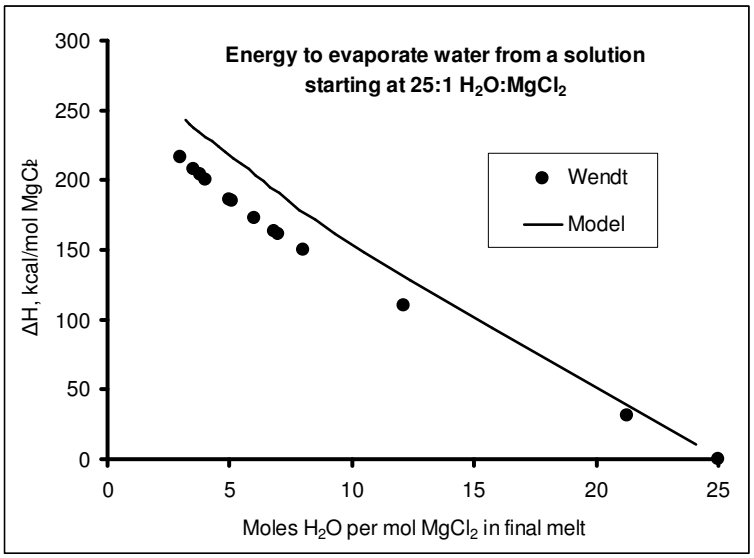

Figure 7 – Evaporation energy versus boiling point

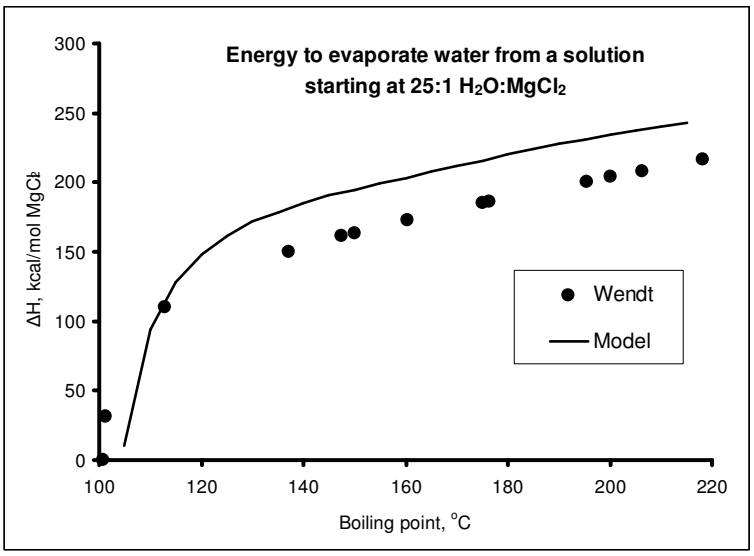

2.3. H_2O-HCl-$MgCl_2$

A publication by Zhang and Zhou presents VLE data for the H_2O-HCl-$MgCl_2$ system[8]. In Figure 8 the symbols are their measured data and the curves were calculated using the AspenPlus® software as calibrated for the H_2O-HCl and H_2O-$MgCl_2$ systems. The volatility of hydrochloric acid increases dramatically as the concentration of magnesium chloride increases because the increased concentration of chloride drives the dissociation reaction for hydrochloric acid towards the formation of molecular HCl. The software over-estimates the volatility of HCl over concentrated $MgCl_2$ solutions somewhat, but the trend is certainly correct.

Figure 8 – VLE of HCl over solutions of $MgCl_2$

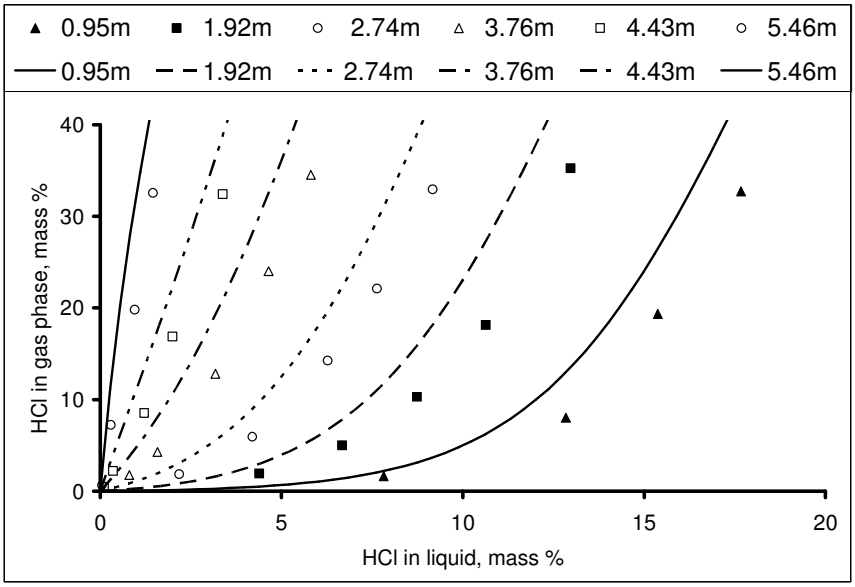

2.4. Application

The purpose of presenting the VLE data for the binary and ternary systems is to show how closely the calibrated AspenPlus® software reproduces the data. In the technology being developed, the system also contains substantial amounts of ferrous and/or ferric iron and lesser amounts, relative to iron and magnesium, of valuable metals such as nickel, copper and cobalt, along with low levels of impurity elements such as zinc and manganese. Measuring the properties of concentrated solutions containing iron and the other elements at elevated temperatures is slated for the immediate future, as part of the overall development. For the work done so far, the approximation used is that these properties are largely determined by the magnesium chloride and the water. The argument for this is that once the hydrolysis of ferric chloride is complete, the liquid phase contains mostly water and magnesium chloride and the vapor phase contains only H_2O because the HCl has been removed, thus the hottest part of the chemistry is actually correctly represented. There will undoubtedly be deviations “en route” between the low- and high-temperature regimes of the circuit, but the properties of the melt at the hottest part of this chemistry can be reasonably assumed to be dominated by magnesium chloride and water. The properties in the lower-temperature parts of the circuit are reasonably well predicted by the thermodynamic correlations in the AspenPlus® software. These assumptions will, of course, be examined and refined as the overall development effort progresses.

3. EXPERIMENTAL

The broader experimental program to generate the data required for the design of the Starfield circuit is presented elsewhere[3]. The hydrolysis step, requiring high temperature and sophisticated laboratory equipment, has only been tested at a semi-continuous (single reactor) scale in the laboratory. So far, this part of the technology is predominantly based on process modeling. At this stage the model is based on the results of an experiment in which a 70:30 mixture by volume of $MgCl_2$ and $FeCl_3$ solutions, each solution containing 260 g/L of total chloride, was heated to

hydrolyze the ferric chloride and drive off the resulting acid. The vapor boiled off was condensed and collected in small increments, each increment being measured and analyzed for HCl. The temperature was recorded, as were the amounts condensed and the corresponding analyses. The results obtained from this experiment are summarized in Figure 9. As the temperature increased, so did both the recovery and concentration of HCl in the vapor driven off. The percentage recovery of hydrochloric acid is based on the chloride associated with the ferric chloride initially present. It is thus also the extent of hydrolysis of the ferric chloride.

Figure 9 – HCl concentration

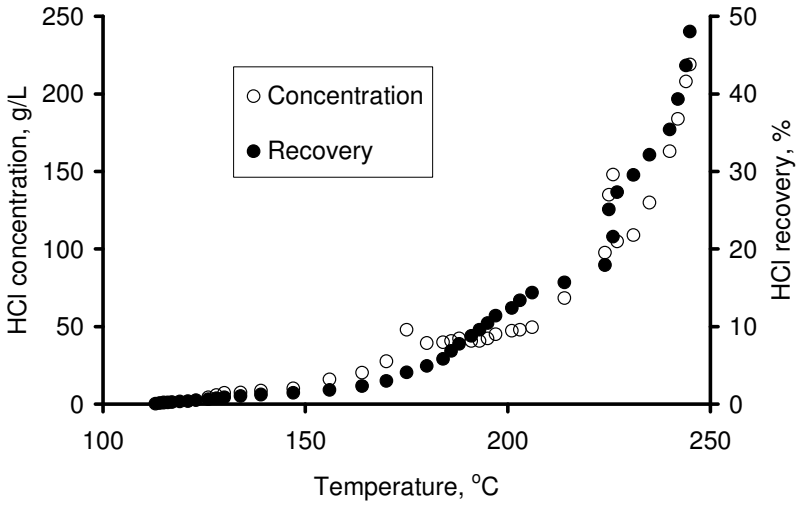

The experiment was simulated using AspenPlus®, initially without adjusting the thermodynamic parameters in the software. The hydrolysis of ferric chloride to hematite and free hydrochloric acid was represented using the following equilibrium reactions (written as shown for simplicity).

$$FeCl_2^+ + Cl^- \leftrightarrow FeCl^{2+} + 2Cl^- \leftrightarrow Fe^{3+} + 3Cl^-$$

$$2Fe^{3+} + 6Cl^- + 3H_2O \leftrightarrow Fe_2O_3\downarrow + 6HCl\uparrow$$

Figure 10 summarizes the results of this exercise. The trend appears to be approximately correct but, as would realistically be expected, the fit of the simulation to the data was not exactly close. Figure 11 shows the results obtained *via* adjusting the model by manipulating the equilibrium constants associated with the formation of the species $FeCl^{2+}$ and $FeCl_2^+$. This gave a significantly better fit of the simulation to the data. The final values used for the two equilibrium constants are given in Table 2, T being Kelvin.

Manipulation of the equilibrium constants for the species $FeCl^{2+}$ and $FeCl_2^+$ has no fundamental basis - the results merely gave the simulation a better fit to the measured data. This will, of course, be revisited when more experimental results become available.

Figure 10 – Fit of the initial simulation to the data

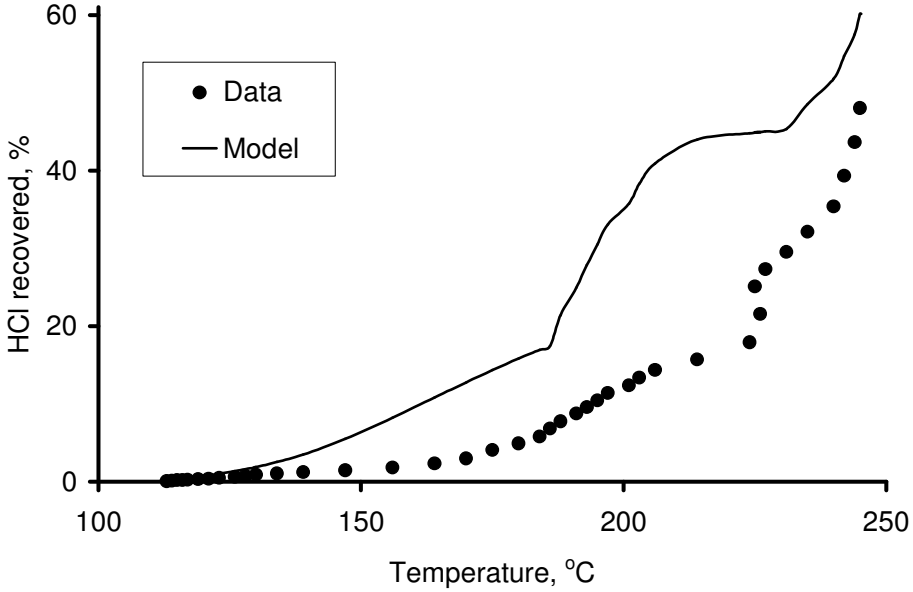

Figure 11 – Fit of the modified simulation to the data

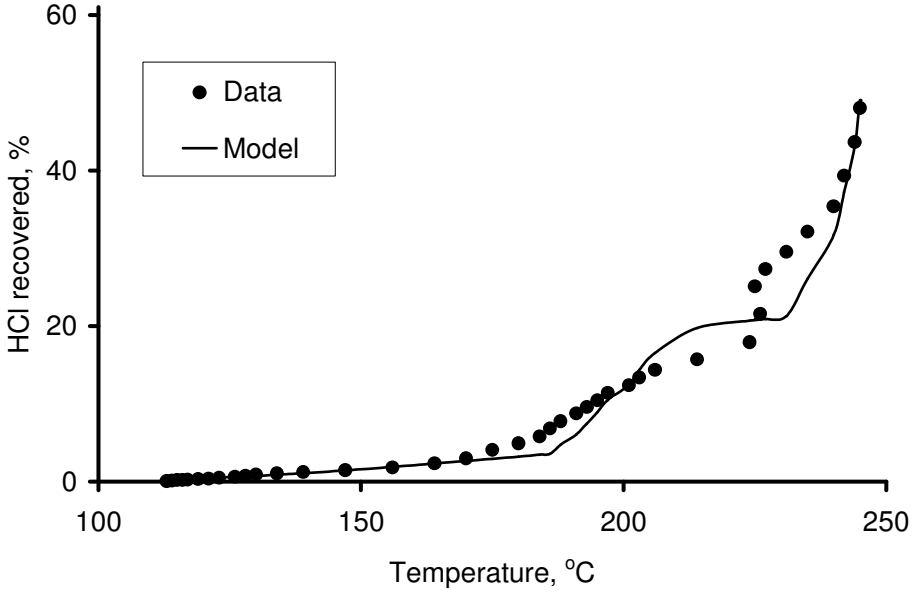

Table 2 – Equilibrium constants for $FeCl^{2+}$ and $FeCl_2^{+}$

Equilibrium reaction	Ln{K} = A - B/T	
$Fe^{3+} + Cl^{-} \leftrightarrow FeCl^{2+}$	A =20.463	B = 4427.4185
$FeCl^{2+} + Cl^{-} \leftrightarrow FeCl_2^{+}$	A =10.708	B = 1992.3383

4. EXTRAPOLATION

The key requirement for the hydrolysis of ferric chloride is to remove the iron from the fluid phase without excessive energy consumption. The experimental results were that even at about 250ºC the total recovery of HCl achieved in the experiment was only about half. Figure 12 illustrates a small process model that was used to explore and extrapolate the experimental results, using the chemical model fitted to the experimental data. The main objective was to predict hydrolysis conditions that achieve essentially complete hydrolysis of the ferric chloride. A secondary objective was to examine the application of steam recompression to the evaporation of water and any free acid ahead of the hydrolysis itself, as an energy saving measure.

In this process model the starting solution is evaporated in two steps, the temperatures in each step being varied to determine whether or not there is an optimal division of the energy load between the two steam compressors and the subsequent hydrolysis section.

Figure 12 – Acid recovery and Fe hydrolysis model

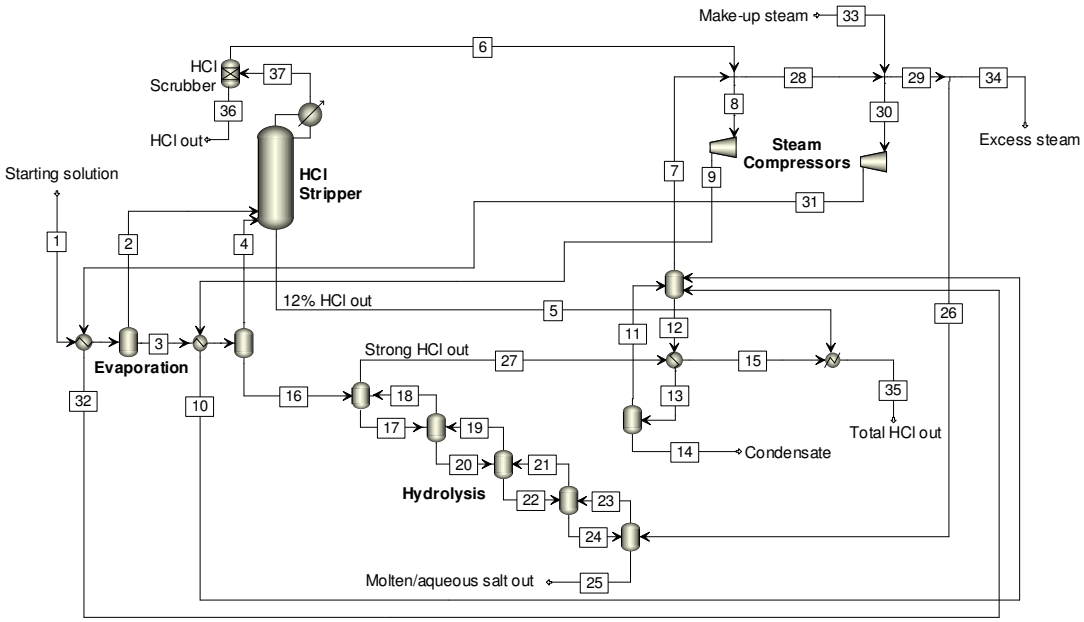

The vapor leaving the two evaporation stages passes through a stripping column in which enough of the water is condensed to capture essentially all the HCl as aqueous hydrochloric acid. The remaining uncondensed steam passes through a scrubber in which any residual acid is removed. The acid-free steam is split and goes to two turbines in which it is compressed to raise its saturation temperature appropriately for re-use as condensing steam on the hot sides of the two heat exchangers in the evaporation section. The model assumes isentropic compression at a thermodynamic efficiency of 72 percent (this being default value in the turbine module in the AspenPlus® software, subject to review in due course).

The concentrated solution leaving the evaporation section goes to the hydrolysis section, where it is heated further and contacted counter-currently in five equilibrium stages with steam at atmospheric pressure to strip out the HCl released as the ferric iron hydrolyzes and precipitates as hematite.

The resulting hot, concentrated steam/acid vapor is cooled and condensed by heat exchange with condensate from the evaporation step, the resulting steam returning to the recompression turbines and any excess condensate leaving the system. The cooled and condensed acid leaves the circuit, as does the magnesium chloride melt and the precipitated hematite.

The input solution is a mixture of $MgCl_2$, $FeCl_3$ and HCl in water, at various concentrations of $FeCl_3$ and $MgCl_2$. The starting concentration of free HCl was arbitrarily chosen as 5 g/L, although this is higher than was achieved in leaching tests done subsequently. The starting concentrations of $FeCl_3$ were chosen as 60, 120 and 180 g/L. The amount of initial magnesium chloride was varied such that the concentration of $MgCl_2$ was 360, 400 or 440 g/L in the input solution. These concentrations were chosen to span the typical composition of solution from leaching tests. The following effects were found.

4.1. Evaporation

Figure 13 shows the calculated elimination of the free HCl initially present in the solution, *versus* the temperature of the solution leaving the evaporation section. According to the model, essentially all of the free acid can be driven off by heating the solution to 140°C. Within the range examined, the exact composition of the initial solution does not affect the elimination of free acid significantly. About 75 percent of the free acid can be removed by heating the solution to between 118ºC and 123ºC and appreciable volatilization of HCl seems to begin at about 115ºC.

Figure 13 – Effect of initial Fe & Mg chloride on free acid recovery

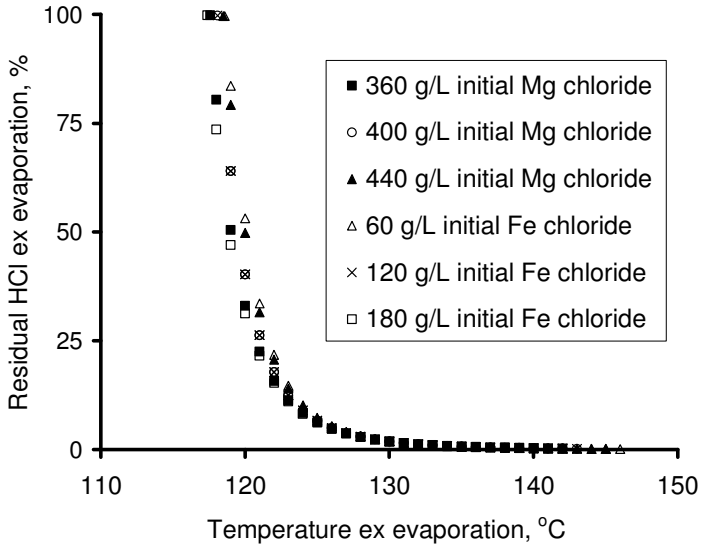

Figure 14 plots the residual water, as a percentage of the concentrated solution, against the exit temperature in the evaporation section. Figure 13 differs from Figure 14 because HCl is more volatile than water in these solutions.

The model predicts a significant rise in the boiling point of the solution as the evaporation of water proceeds. The higher the boiling point elevation, the higher the pressure to which the steam evaporated from the solution must be recompressed to give it the temperature required to drive the

evaporation. The greater the steam pressure required, the greater the energy required to drive the recompression equipment.

Figure 14 – Residual water ex evaporation

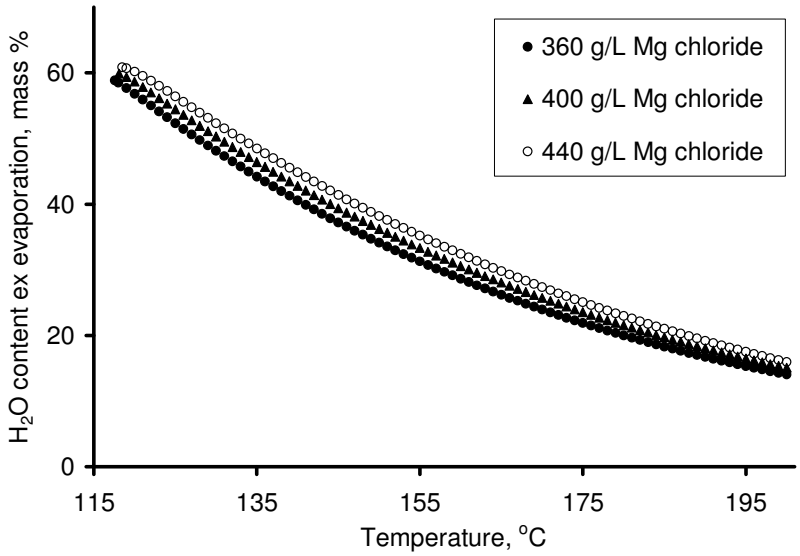

4.2. Hydrolysis

Figure 15 shows the predicted effect of hydrolysis temperature on the extent of hydrolysis and the corresponding strength of the liberated HCl, for a case in which the evaporation section was taken to just short of the start of hydrolysis and the hydrolysis is carried out in a single stage. According to the model, both the extent of hydrolysis and the concentration of the acid liberated peak at about 235°C, in this case.

Figure 15 – Effect of hydrolysis temperature

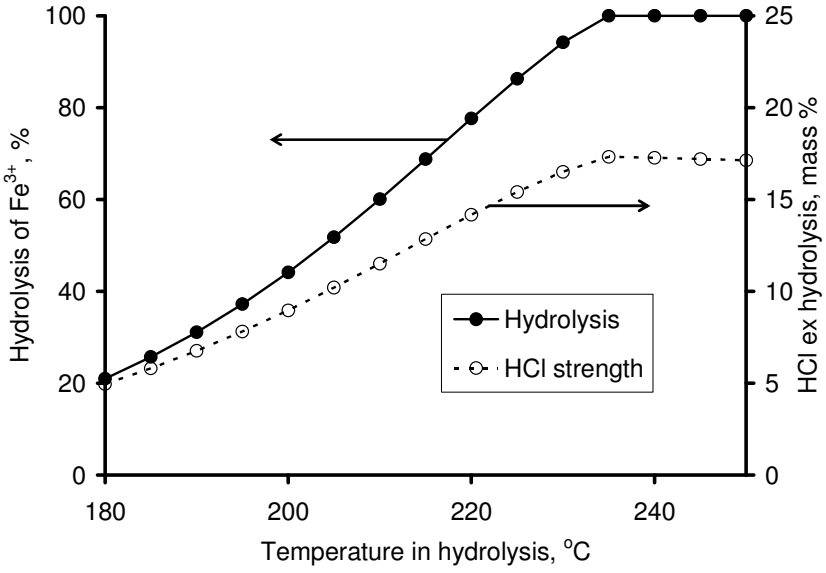

A parameter that could also be varied is the partial pressure of HCl above the molten phase. A steam purge would remove the HCl, thereby lowering its partial pressure over the liquid phase and

so driving the extent of hydrolysis further. It would also raise the partial pressure of water vapor above the melt and thus the activity of water in the melt, moving the hydrolysis equilibrium towards hematite. Figure 16 shows the effect of the amount of purge steam on the predicted extent of hydrolysis and the strength of the acid recovered. The open symbols denote the acid strength and the solid symbols the extent of hydrolysis. In this example, the temperature in the second evaporation step was 180°C and the temperature in the hydrolysis section was 250°C. In this case the strength of the acid liberated is almost double that of the case shown in Figure 15. At an exit temperature from the evaporation section of 180°C, significantly more water is driven off and some hydrolysis occurs in the evaporation section. The overall effect is a little less, but more concentrated, acid leaving the hydrolysis train. Less water into the hydrolysis train means less steam out, hence more concentrated acid out.

Figure 16 – Effect of purge steam on hydrolysis

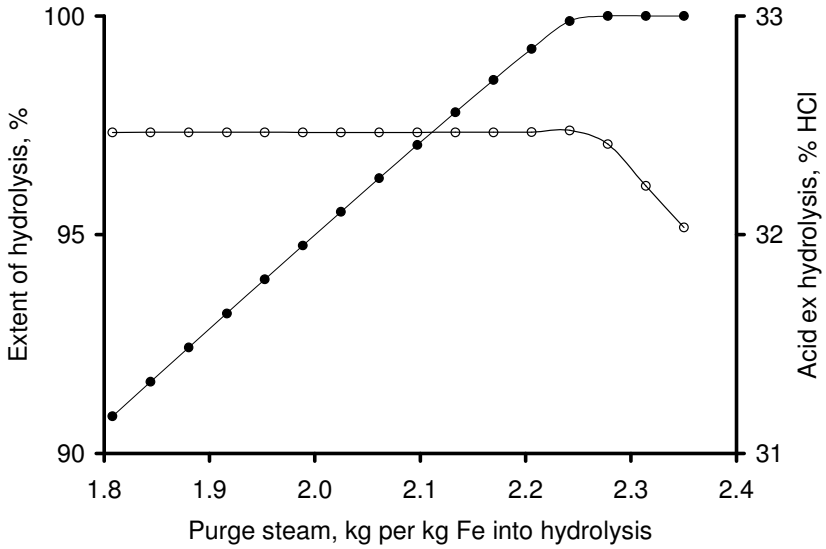

Figure 17 – Hydrolysis versus HCl pressure

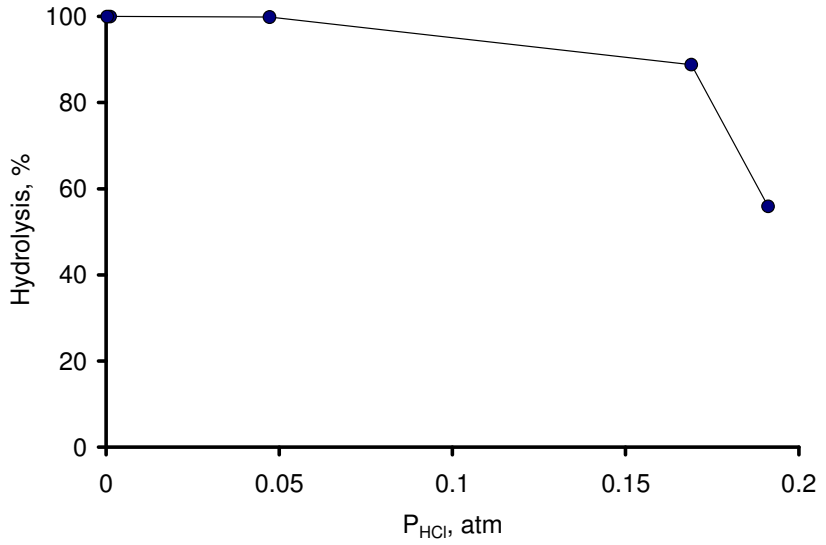

Figure 17 shows the calculated effect of HCl partial pressure on the extent of hydrolysis, for the same example as shown in Figure 16. It would appear that the higher partial pressures of HCl over the liquid phase limit the extent of hydrolysis. These calculations suggest that the extent of the ferric hydrolysis reaction depends on temperature and the composition of the vapor phase. This would explain why the experiment on which the model was based did not achieve complete hydrolysis – the partial pressure of HCl above the liquid phase was too high. Had a purge of steam or other gas been passed through the reactor, the partial pressure of HCl over the liquid phase would have been reduced, which would have driven the hydrolysis reaction significantly further towards completion.

4.3. Energy

The total energy demand is the sum of the energy needed for evaporation and hydrolysis. An example of the predicted total energy requirement is shown in Figure 18, assuming two steam recompression turbines (one for each step, as illustrated in Figure 12) in the evaporation section. This curve is for an exit temperature of 170°C from the evaporation section and the x-axis is the intermediate temperature in the evaporation section. In this case the starting solution contained 120 g/L $FeCl_3$, 360 g/L $MgCl_2$ and 5 g/L HCl and the overall energy demand would be minimized by operating the first step of the evaporation section at 135° to 140°C.

Figure 18 – Energy demand for evaporation and hydrolysis

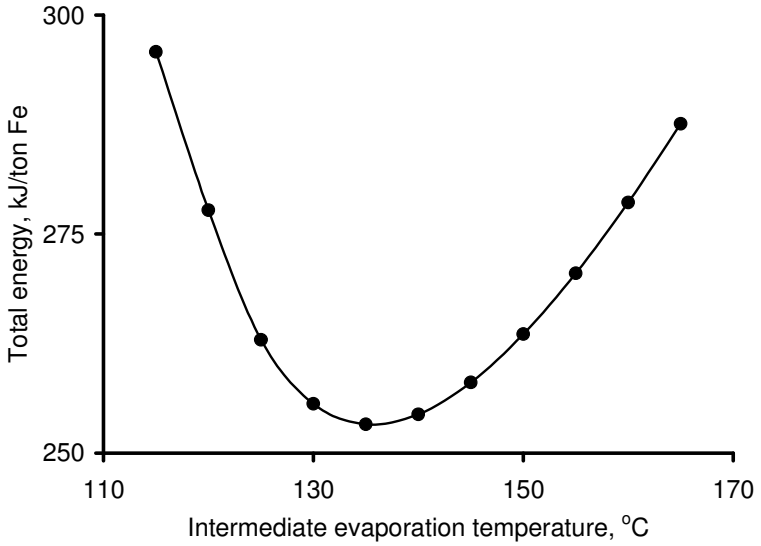

Figure 19 shows the effects of the composition of the starting solution on the combined energy requirements of the evaporation and hydrolysis sections, assuming methane-fired turbines driving the steam recompression turbines and that the energy for the hydrolysis section is supplied by direct combustion of methane. These curves assume input concentrations of 60, 120 and 180 g/L $FeCl_3$, 360, 400 and 440 g/L $MgCl_2$ and 5 g/L HCl. Each curve is the one giving the minimum total fuel requirement for the associated starting solution.

Figure 20 summarizes similar information to Figure 19, but assuming that all the energy required for evaporation and hydrolysis is derived directly from the combustion of methane.

Figure 19 – Fuel demand with steam recompression

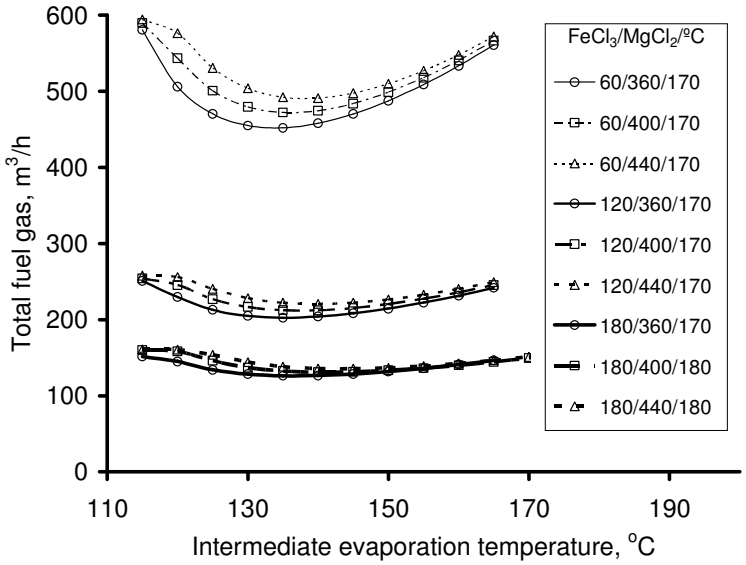

Figure 20 – Fuel demand without steam compression

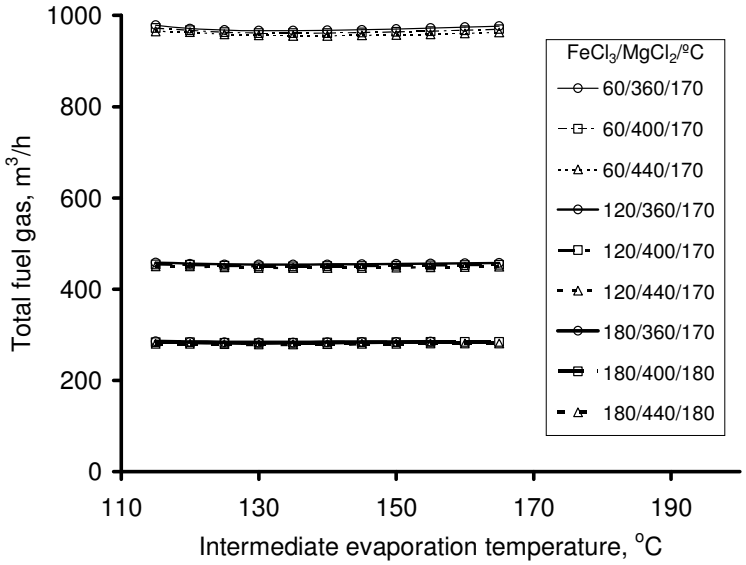

The strongest effect on the overall fuel requirement is the starting concentration of ferric chloride. This would be expected, because higher starting ferric chloride corresponds to leaching at a higher solid-to-liquid ratio, hence less water to evaporate per unit mass of solids leached. The effect of the input concentration of magnesium chloride on the fuel demand appears to be much weaker than that of ferric chloride.

Recompressing steam in the evaporation section appears to require about half the fuel required were all the energy to be supplied by simply burning methane. This would appear to justify the inclusion of steam recompression in the Starfield circuit - subject, naturally, to its impact on the overall cost of the technology *via* its contribution to the capital cost.

5. APPLICATION

The Starfield circuit has evolved through a few configurations, the one illustrated in Figure 21 being recent but probably not the ultimate design. The major unit operations in the circuit are non-oxidative and oxidative leaching, evaporation, oxidation of ferrous iron, more evaporation, hydrolysis, quenching and re-dilution of the melt/hematite slurry, filtration and washing of the hematite. Separation of the Ni, Cu, Co, Mn, and Zn from the solution *ex* the oxidative leach is done by anion exchange, loading them onto the resin as the anionic chloro-complexes complexes that form in high-chloride brine and generating a raffinate containing the nickel, which does not form anionic chloro-complexes. The resin is stripped with water, dissociating the metal chloro-complexes and generating a low-chloride eluate containing the Cu, Co, *etc.* as cations. The base metals are recovered from the raffinate and the eluate by cation exchange and electrolysis.

Figure 21 – Starfield circuit

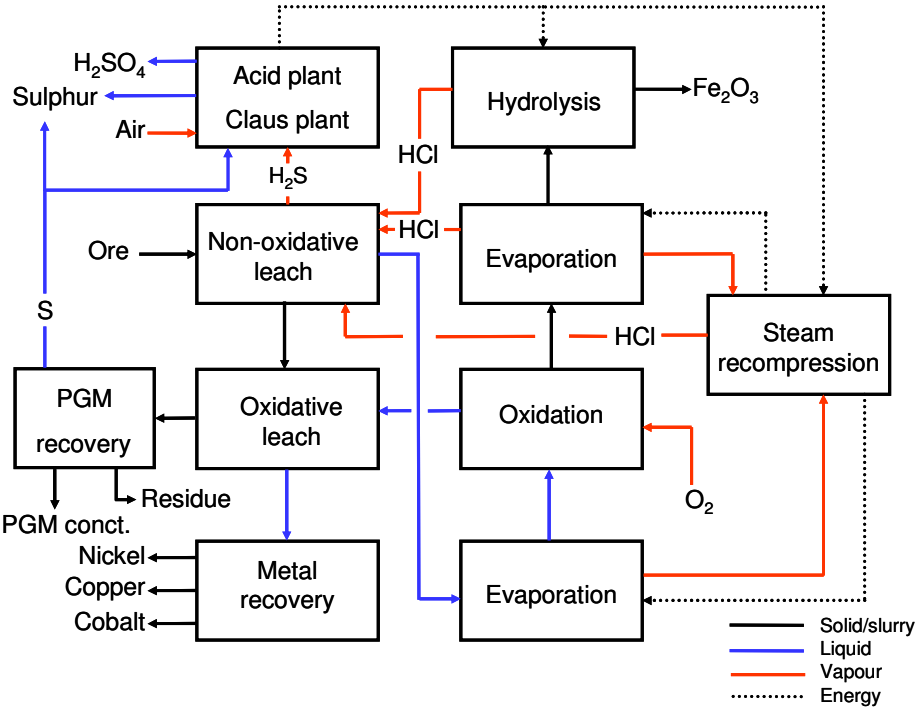

Table 3 gives the mineral assemblage used to represent the incoming ore. The bulk of the material is pyrrhotite. Table 4 lists the main reactions occurring in the process. The anion exchange section uses recycled condensate as the eluant. After the removal of copper and cobalt from the eluate by cation exchange and electrolysis, that water is used to quench the melt from the hydrolysis section so that the hematite can be removed by filtration and washing and the magnesium chloride can be efficiently recovered and recycled to the leach. The water added in these steps has to be evaporated as the brine moves from the leach to the hydrolysis section, which makes the process intrinsically energy intensive.

The three sources of energy in the Starfield circuit are the heat of reaction emanating from the conversion of the H_2S from the non-oxidative leach to sulphuric acid, reuse of the latent heat in the evaporated water *via* the recompression of low pressure steam and the recovery of waste heat.

Table 3 – Starfield ore

Mineral	Mass %	Mineral	Mass %
(Pt, Pd)S	2 ppm	SiO_2	15.0
NiS	0.9	$FeSiO_3$	1.3
CoS	0.1	$MgSiO_3$	1.8
CoS_2	0.04	$MnSiO_3$	0.1
FeS	6.7	$ZnSiO_3$	0.01
$CuFeS_2$	2.5	Na_2SiO_3	0.1
Fe_7S_8	70.3	$CaSiO_3$	0.6
Al_2O_3	0.5	K_2SiO_3	0.1

Table 4 – Main reactions

Primary leach
$Fe_7S_8 + 14H^+ \rightarrow 7Fe^{2+} + 7H_2S + S$
Secondary leach
$NiS + 2Fe^{3+} \rightarrow Ni^{2+} + 2Fe^{2+} + S$
$CuFeS_2 + 4Fe^{3+} \rightarrow Cu^{2+} + 5Fe^{2+} + 2S$
$CoS + 2Fe^{3+} \rightarrow Co^{2+} + 2Fe^{2+} + S$
Oxidation
$6Fe^{2+} + 1½O_2 \rightarrow Fe_2O_3 + 4Fe^{3+}$
Hydrolysis
$2Fe^{3+} + 3H_2O + 6Cl^- \rightarrow Fe_2O_3 + 6HCl$
Acid plant
$H_2S + 2O_2 \rightarrow H_2SO_4$
Anion exchange (M=Cu, Co, Mn, Zn)
$MCl_3^- + Resin•Cl \rightarrow Resin•CuCl_3 + Cl^-$
$Resin•MCl_3 \rightarrow Resin•Cl + M^{2+} + 2Cl^-$
Cation exchange and electrolysis (M = Ni, Cu, Co)
$2Resin•H + M^{2+} \rightarrow Resin_2•M + 2H^+$
$Resin_2•M + 2H^+ \rightarrow 2Resin•H + M^{2+}$
$M^{2+} + H_2O \rightarrow M^0 + 2H^+ + ½O_2$

5.1. Recompression of steam

Technology by which the latent heat of evaporated water can be reused is the recompression of low pressure steam to high enough pressure for its saturation temperature to be raised sufficiently for it to be used as a heating medium. Figure 22 illustrates one way of arranging this. In this illustration, recompressed steam is used to evaporate the incoming brine, generating concentrated brine and H_2O/HCl vapor that leaves the evaporator at the boiling point of the concentrated brine. Once the acid has been scrubbed from this vapor, its condensation temperature becomes that of

water (100°C at atmospheric pressure). The condensate from the brine evaporation step is flashed to a lower pressure, such that the temperature of the resulting condensate and steam is lower than the condensation temperature of the steam evaporated from the brine, after the acid has been scrubbed out. The temperature chosen is 85°C, at which temperature the absolute pressure is 0.58 Bar. The low-pressure condensate, its evaporation temperature being 85°C, can be re-evaporated by heat exchange with the acid/steam from the brine evaporation step and/or other convenient process streams. The resulting low-pressure steam is combined with the low pressure steam from the flash step and recompressed to a pressure sufficient to raise its saturation temperature above the boiling point of the concentrated brine and returned to the condensing side of the evaporator.

Figure 22 – Evaporation using steam recompression

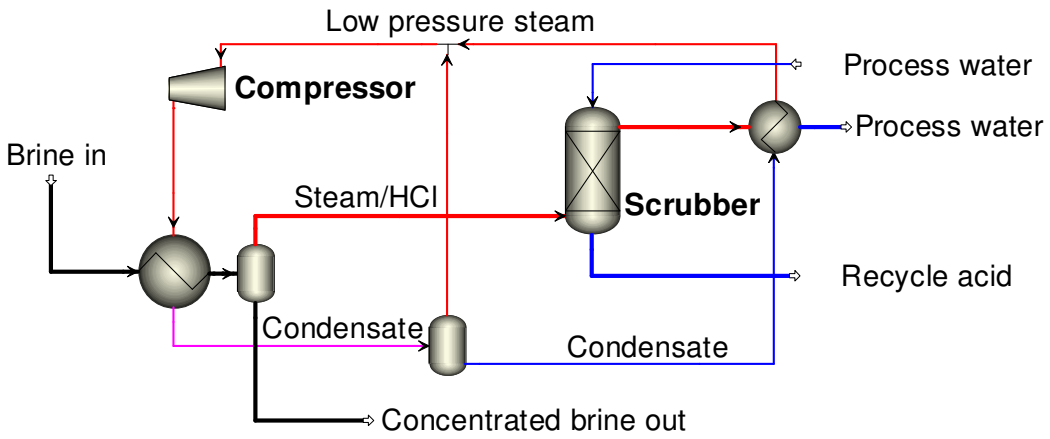

The reason for this particular configuration is that even though the H_2O/HCl vapor evaporated from the brine is scrubbed with water to remove acid and is theoretically free of acid, recompressing that steam would entail a risk of acid reaching the compressor and causing corrosion problems. Using a closed loop of pure steam/condensate ensures that the compressor cannot be exposed to acid. The heat exchangers, not having moving parts, can be much more easily made from acid resistant materials than the compressor.

5.2. Energy from the acid plant

In acid plants burning hydrogen sulphide there is a variation called a “wet gas plant” in which the H_2O/SO_2 gas from the combustion chamber goes directly to the catalytic conversion reactors with no intermediate drying and the resulting gaseous SO_3/H_2O is condensed into concentrated sulphuric acid[9]. The Starfield circuit uses this variation because it maximizes the amount of high pressure steam generated. Figure 23 illustrates the arrangement selected for extracting mechanical and thermal energy from the heat of reaction emanating from the conversion of H_2S to H_2SO_4. The hydrogen sulphide is burned in air and the resulting hot H_2O/SO_2 bearing gas is used to superheat recycled medium pressure steam and to generate superheated high pressure steam. The H_2O/SO_2 gas leaving the boiler is contacted with more air in a catalytic conversion reactor, converting the SO_2 to SO_3 and releasing more heat that is captured by counter-current partial evaporation of recycled high pressure condensate. The H_2O/SO_3 is converted into concentrated

liquid H_2SO_4 in the absorber, releasing more heat that is also captured by partial evaporation of the high pressure condensate. The remaining gas is vented and the concentrated sulphuric acid leaves the circuit.

Figure 23 – Energy recovery from H_2S combustion

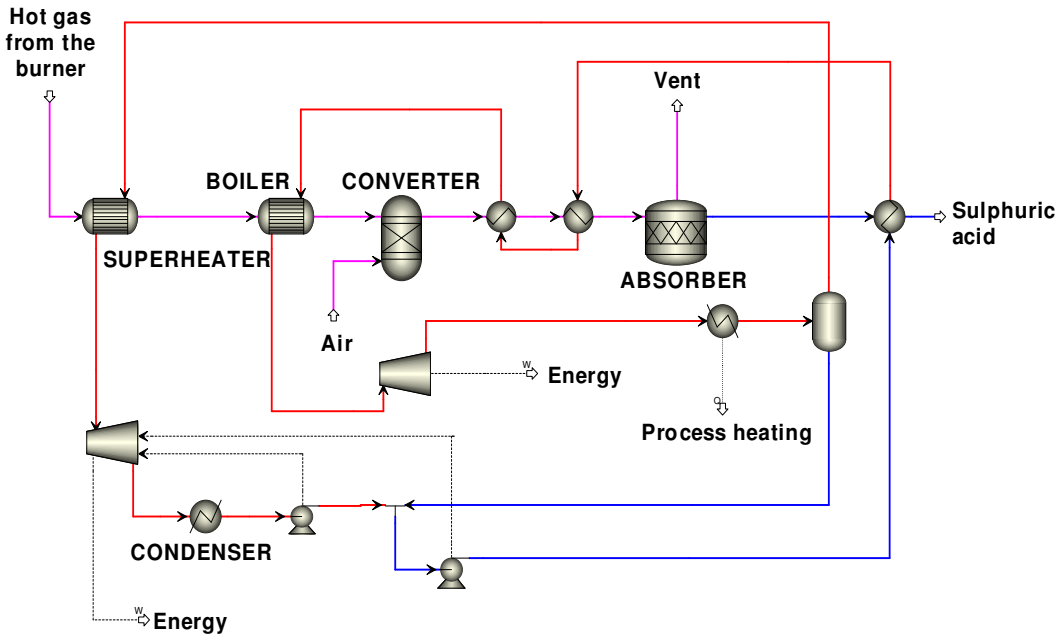

The boiler produces superheated high-pressure steam (457°C and 56.5 Bar abs)[10]. This steam is expanded to 28 Bar absolute through a turbine, generating mechanical energy. The saturation temperature of steam at that pressure (28 Bar absolute) is 230°C, so it is hot enough to supply its heat of condensation to the hydrolysis section (operating at about 200°C) and the evaporation sections (operating at lower temperatures) of the process. The heat loads in the circuit condense the bulk of the 28 Bar steam. The residual 28 Bar steam is separated in a flash vessel and recycled to the superheater. The condensate is pumped to 56.5 Bar absolute and recycled to the boiler *via* the counter-current heat exchange train associated with the catalytic converter and the absorber.

The superheater heats the recycled 28 Bar steam to 460°C and that superheated steam is expanded to 0.05 Bar absolute in a second turbine, generating more mechanical energy. The low-pressure steam leaving this turbine is condensed at 30°C and the condensate is pumped back to 28 Bar absolute, at which pressure it rejoins the other condensate and is recycled.

5.3. Recovery of waste heat

The sources of waste energy in the circuit are the following.

- Steam/condensate from the evaporation steps after it has been used to evaporate low-pressure condensate in the steam recompression loop is cooled to 50°C.
- The spent oxygen leaving the oxidation section, after it has been used to evaporate condensate in the second steam recompression loop, is cooled to 50°C.

- The hot sulphuric acid leaving the acid plant is cooled from 230°C to 50°C.
- Quenching the melt after hydrolysis requires cooling to bring the temperature of the quenched brine/hematite slurry down to 100°C.
- The hot solution leaving the oxidative leach en route to the ion exchange and electrolysis steps has to be cooled from about 120°C to 80°C to avoid destroying the resin.
- The H_2S/HCl/steam leaving the non-oxidative leach is cooled to its dew point before being scrubbed with process water to remove volatilized HCl.
- The H_2S/steam leaving the acid scrubber after the non-oxidative leach is cooled to 50°C to condense out most of the water. Cooling this stream to 90°C in a first step condenses much of the water and allows the capture of the associated latent heat.

All this cooling is done by the evaporation of recycled condensate at sub-atmospheric pressure, as illustrated in Figure 24.

Figure 24 – Waste heat recovery

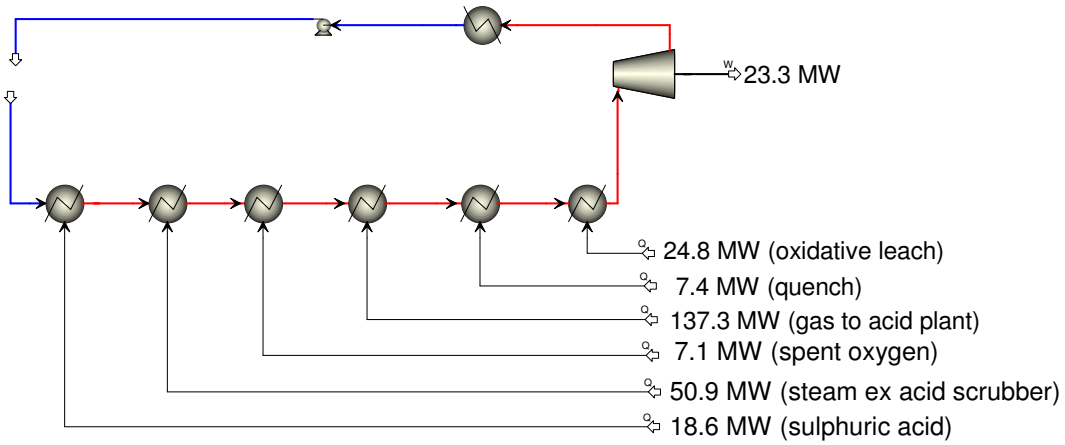

The pressure chosen is 0.58 bar absolute, at which pressure water boils at close to 85°C, which maintains a thermal driving force for the heat exchange steps of at least 5°C. The resulting 0.58 Bar steam is expanded to 0.05 Bar absolute through a turbine to generate mechanical energy. The exhaust steam is condensed at 30°C and the condensate is pumped back up to 0.58 Bar absolute and recycled. In Figure 24 the dotted lines denote the various cooling loads and the numbers next to each dotted line are the calculated cooling duties. The mechanical energy recovered is only about ten percent of the combined cooling load, but is still significant compared to the energy requirements presented next.

5.4. Results

The configuration selected as the Starfield base case has all the H_2S from the leach converted to sulphuric acid, while the elemental sulphur and precious metals in the secondary leach residue are stored for future exploitation. The annual tonnages of base metals, byproducts and residues are as listed in Table 5. Table 6 lists the annual consumption of ore and reagents. Table 7 lists the annual consumption of water.

Table 5 – Annual production, tons

Nickel metal	12 322
Copper metal	17 497
Cobalt metal	1 027
Sulphuric acid	1 564 353
Hematite	1 421 035
Gangue residue plus sulphur	577 806

Table 6 – Annual ore and reagent consumptions, tons

Ore into the primary leach	2 100 000
Magnesium chloride, as $MgCl_2$	4 629
Oxygen, as 100% O_2	201 838
Sulphuric acid, as 100% H_2SO_4	3 631
Hydrochloric acid, as 100% HCl	10 676

Table 7 – Annual water consumptions, tons

Boiler feed water	252 000
Process water	853 950
Cooling water make-up	5 389 819

Table 8 summarizes the calculated power consumption in the circuit. The first two numbers come from the process model and the values for mining, milling, the oxygen plant and general pumping and agitation in the circuit were taken from the preliminary engineering assessment[4].

Table 8 – Power consumption, MW

Evaporation compressor 1	4.2
Evaporation compressor 2	5.4
Power for mining	6.0
Power for drying and milling the ore	7.4
Power for the oxygen plant	6.4
Power for electrolysis	10.6
Power for pumping, agitation etc.	5.3

Table 9 lists the power generated in the acid plant and from waste heat in the circuit, along with the total consumption and the surplus power that would be available for export.

Table 9 – Power generation, MW

Net power from the acid plant	23.5
Power from waste heat recovery	26.4
Power consumption in the process	45.3
Surplus power from process	**4.6**

The ninety percent of the waste heat not converted into mechanical energy (and thence into electrical power) emerges as warm water that would conventionally be cooled and recycled as is normal with cooling water. It might also be possible too use this water as a source of low-grade energy for space heating or other creative applications, given the frigid location of the project.

6. CONCLUSIONS

The process model, as developed to date, predicts that the envisaged circuit will be self-sufficient in energy, and even able to export a small surplus. The circuit will operate without the combustion of fossil fuel (apart from start-up and emergency conditions), and the surplus power exported will displace other power generated from fossil fuel. This gives the circuit a negative carbon footprint.

The modeling approach adopted for this work enabled detailed evaluation of various configurations of unit operations and operating conditions and substantially enhanced the overall understanding of the circuit. At the present state of knowledge, the circuit shown in Figure 21 is thought to be close to optimal, but it will be re-examined when more experimental results become available.

The circuit is complex because of the need for extensive recycling of energy. Process modeling is likely to remain an important contributor to the overall development effort. While prematurely believing the numbers emanating from any model is always unwise, correctly applied process modeling, combined with the right experimental work and careful review, is a very powerful tool in the development of complex processes such as the Starfield circuit.

7. ACKNOWLEDGEMENT

Permission from the management team of Starfield Resources Inc. to publish this paper is gratefully acknowledged. The extensive and intensive efforts of Bryn Harris of NeoFerric Technologies Inc. and Phil Evans of Andeburg Consulting Services in evaluating the results of the modeling work is also gratefully acknowledged.

8. REFERENCES

1. 1. G.B. Harris, C.W. White and G.P. Demopoulos. *Iron Control in High Concentration Chloride Leach Processes*. Iron Control Technologies (J.E. Dutrizac and P.A. Riveros, Editors), Proceedings of the Third International Symposium on Iron Control in Hydrometallurgy, 36th Annual CIM Hydrometallurgical Meeting, Montreal, October 1-4, 2006, p. 445.

2. 2. G.B. Harris, C.W. White, G.P. Demopoulos and B. Ballantyne. *Recovery of Copper from a Massive Polymetallic Sulphide by High Concentration Chloride Leaching*. Proceedings of the John E. Dutrizac Symposium on Copper Hydrometallurgy (P.A. Riveros, D.G. Dixon, D.B. Dreisinger and M.J. Collins, Editors), Volume IV of Copper 2007, Sixth International Copper-Cobre Conference, Toronto, August 25-30, 2007, p. 21.

3. 3. Bryn Harris and Carl White. *Recent developments in the High-Strength Chloride Leaching of Base Metal Sulphide Ores*. This conference, ALTA Ni/Co 2008.

4. 4. *Preliminary Assessment of the Ferguson lake project, Nunavut territory, Canada. Prepared for Starfield resources Inc. NI 43-101 report*. http://www.sedar.com/CheckCode.do;jsessionid=0000cSmeZk3sNum6zWJJvQySlI2:-1

5. 5. *Kirk Othmer Encycopaedia of Chemical technology*.

6. 6. C. H. Wendt, Auxon Corporation, 31 Bagley Court, Madison WI 53705 and D.P. Butt, K.S. Lackner and H-J Ziock, Los Alamos National Laboratory, Los Alamos, NM 87545. *Thermodynamic Calculations for Acid Decomposition of Serpentine and Olivine in $MgCl_2$ Melts, Part I. Description of Concentrated $MgCl_2$ Melts, July 27, 1998*. . LA-UR-98-4528.

7. 7. H.-H Emons, W. Voigt and F. –W Wollny. *Dampfdrukmessungen am System magnesiumchlorid-Wasser*, Z. phys. Chemie, Leipzig 267 (1986), pp. 1-8. Cited by Wendt *et al*.

8. 8. Zhang, Y. and Zhou, R. *Vapor-Liquid Equilibria for Water+Hydrochloric Acid+Magnesium Chloride and Water+Hydrochloric Acid+Calcium Chloride Systems at Atmospheric Pressure*. Chinese J. Chem. Eng., 14(2) 276-280 (2006).

9. 9. *United States Patent 5118490*

10. 10. Information from Haldor Topsoe.